IMPROVING CRITICAL SPEED CALCULATIONS USING FLEXIBLE BEARING SUPPORT FRF COMPLIANCE DATA

by

John C. Nicholas

Head, Rotordynamics Group

John K. Whalen

Analytical Engineer, Rotordynamics

and

Sean D. Franklin

Analytical Engineer, Stress Analysis

Advanced Engineering Department

Dresser-Rand Company

**Steam Turbine, Motor & Generator Division**

Wellsville, New York

John C. Nicholas received his B.S.A.E. degree from the University of Pittsburgh (1968), his M.S.M.E. degree from Northwestern University (1969), and his Ph. D. degree (1977) from the University of Virginia in rotor-bearing dynamics. While at Virginia, he authored the tilting pad and pressure dam bearing computer programs that are used by many rotating equipment vendors and users.

Dr. Nicholas has worked in the rotating equipment industry for the last eight years in the rotordynamics area, after teaching at Virginia for one year. Since 1983, he has been Head of the Rotordynamics Group at Dresser-Rand in Wellsville. He is responsible for all of the rotor and bearing dynamics for the division. Recently, his research efforts have been concerned with support flexibility effects on rotordynamic calculations.

Dr. Nicholas, a member of ASME, ASLE, and the Vibration Institute, has authored more than 20 technical papers in rotorbearing dynamics. He also holds a patent in the U.S. and Canada for fluid film pocket bearing.
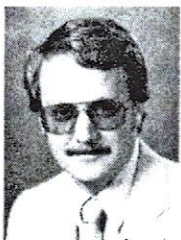
John K. Whalen is an Analytical Engineer in the Rotordynamics Group of Dresser-Rand, Wellsville.

Mr. Whalen graduated from the Rochester Institute of Technology with a B.S.M.E. degree (1981). He is currently studying for an M.S.M.E. from RIT. His professional experience includes three years as a Product Engineer in the Engineered Product Group and two years as an Analytical Engineer in the Rotordynamics Group. Current job responsibilities include complete rotordynamics analyses of all production steam turbine and generator rotors.

Mr. Whalen is a member of ASME.

Sean D. Franklin is an Analytical Engineer with the Stress Analysis Group of Dresser-Rand Company, in Wellsville, New York.

Mr. Franklin graduated from Clarkson College of Technology in 1980. His experience includes six years of stress and vibration analysis, using classical and finite element methods and modal testing. He has experience in vibration testing of components of steam turbines and other rotating equipment.

ABSTRACT

The importance of including flexible supports in rotordynamic analyses is discussed. Various methods of including the support in rotordynamic calculations are reviewed. A method is described in which actual compliance frequency response function, FRF, data are used directly in a rotordynamic forced response computer program to accurately predict a steam turbine rotor's critical speed. The flexible support model is described as two single degree of freedom, SDOF, spring-mass-damper systems per bearing support. The methodology of acquiring the FRF data via impact hammer testing is described, and the equations are summarized that incorporate the FRF data into the flexible support model. Three flexible support models of increasing sophistication are used to analytically predict the rotor and support resonances. These results are compared to the actual steam turbine speed-amplitude plots. Modelling the support as many speed dependent SDOF systems accurately predicts the location of the rotor's first critical speed and also the split critical peaks and several support resonance speeds.

INTRODUCTION

It has become increasingly important in recent years to accurately predict the location of rotor lateral critical speeds. Most of this emphasis is due in part to the stringent rotordynamics user specifications to which rotating equipment manufacturers must adhere. This is particularly true for the petrochemical

industry where a typical standard prohibits critical speeds to be located between 15 percent below the minimum speed to 20 percent above the maximum continuous speed [1].

The same standard limits critical speed amplification factors to be below 8.0, while stating that amplification factors below 5.0 are preferable. As the amplification factor decreases, the critical speed becomes less severe, with a much more gradual change in vibration amplitude with speed. This type of design requires the rotor shaft to be relatively rigid to permit sufficient shaft movement at the bearings thereby allowing the bearing damping to be effective in vibration suppression. Furthermore, the bearing flexibility plays a predominant role in locating the rotor's critical speed. For flexible shaft rotors with higher amplification factors, critical speeds can be accurately predicted by carefully modelling the shaft. The bearing flexibility plays a very small role in locating the critical speed.

Thus, for low amplification factor rotors, critical speeds are less severe, but are much more difficult to predict analytically, since they depend greatly on the stiffness and damping properties of the bearing fluid film and the bearing supporting structure. This support includes the pad and pad pivots for tilting pad bearings, the bearing housing, the housing support feet, the baseplate and the foundation.

The flexibility of the bearing support beyond the fluid film can dramatically alter the effective bearing stiffness and damping properties acting on the rotating shaft [2, 3, 4]. The analysis of machine vibration response based on rigid bearing supports predict critical speeds that are substantially higher than actual values [2, 3]. Nicholas and Barrett [2] found that for the four rotors analyzed, neglecting support flexibility resulted in predicted first critical errors that range from 14 percent to 21 percent high and second critical errors that range from 40 percent to 88 percent high. Since rotating machinery is designed, marketed and sold, for the most part, based on analytical prediction, an accurate method of easily incorporating the support flexibility effect into rotordynamic analyses is of paramount importance.

To this end, several researchers have included the effects of support flexibility into rotordynamic analyses. The method usually used is to model the supports with stiffness and damping coefficients which are constant over the entire speed range [2, 5, 6, 7, 8]. In most cases, the support stiffness is based on static deflections of the bearing pedestal (experimentally and/or analytically calculated). This method also requires values for the support mass and damping which require additional calculations and approximations. While this approach can be successfully utilized to predict both the location and amplification of rotor critical speeds [2], it will not show more than a single support or foundation resonance.

Recently, detailed models of support structures have been incorporated into rotordynamic analyses in an effort to predict the support-rotor resonance interactions. The usual approach has been to use either an approximate beam model [9] or a modal model from finite element analysis of the structure [10, 11, 12]. Some studies use component mode synthesis techniques [10, 11] whereas Queitzsch [12] uses analytical frequency response functions (FRF) to represent the supporting structure. These methods have proven successful, but they are time-consuming and costly.

The method proposed here utilizes experimental FRF data to represent the bearing support structure. The experimental data is determined from modal analysis techniques where the response of the structure to a known force is recorded. The resulting FRF data, both magnitude and phase, are plotted as a function of frequency. If the magnitude of the FRF function is displacement divided by the force, the resulting data is called dynamic compliance [13].

The application of experimental FRF data to rotordynamic analyses has been discussed previously [3, 14, 15]. One of the biggest advantages of this method is that the support mass and damping is included implicitly in the FRF data along with the support stiffness. The FRF data can easily be incorporated into the rotordynamic support model used in references [2, 5, 6, 7], either as a constant dynamic stiffness over a narrow speed range or as a speed dependent dynamic stiffness over the entire speed range.

The modal analysis technique used in determining the dynamic compliance data is detailed herein. The data is then employed in a forced response rotordynamic analysis, using various levels of flexible support model sophistication. The results will be compared to actual test stand speed amplitude plots from a steam turbine, running on the test stand with a known midspan unbalance.

FLEXIBLE SUPPORT MODEL

A typical outline drawing of a steam turbine case is shown in Figure 1. The steam end bearing is housed in a bearing case that is supported by a flex plate to allow for axial thermal expansion. The exhaust end bearing case is supported within the exhaust casing which sits on two sets of thick horizontal plates with gussets for added stiffness. These plates along with the flex plate are attached to the baseplate.
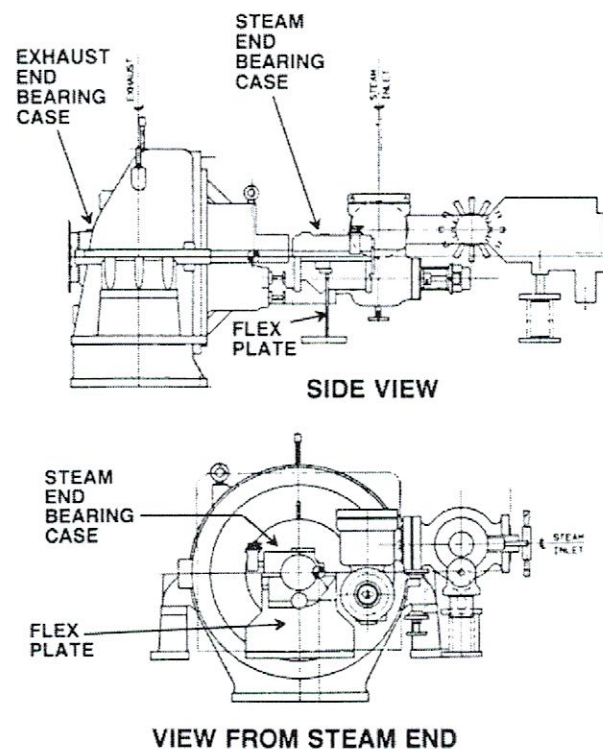

Figure 1. Steam Turbine Outline Drawing Showing Exhaust and Steam End Bearing Cases and Supports.

A model for this complex support is illustrated in Figure 2. The first level of flexibility is the bearing fluid film which is represented by eight principal (XX, YY) and cross-coupled (XY, YX) stiffness and damping coefficients. For tilt pad bearings, the second level of flexibility is the pad and the pad pivot. This effect may be accounted for in the tilting pad bearing analysis [2, 4, 14]. The next level of flexibility is everything past the pad pivot. This includes the bearing case, the supporting plates and the

baseplate. Again, the support may be modeled by eight principal and cross-coupled stiffness and damping coefficients along with the support mass.
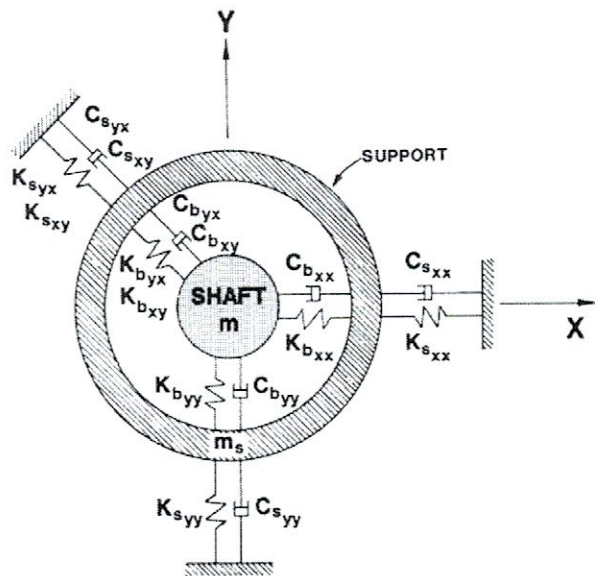

Figure 2. Bearing Fluid Film and a Single Two Degree of Freedom Flexible Support Model.

Further support model simplification is shown in Figure 3. The single support mass with two degrees of freedom illustrated in Figure 2 is reduced to two single degrees of freedom (SDOF) support spring-mass-damper systems in both the horizontal X and vertical Y directions. Only the Y direction for illustrative purposes is considered in Figure 3, but an identical system also exists for the X direction.
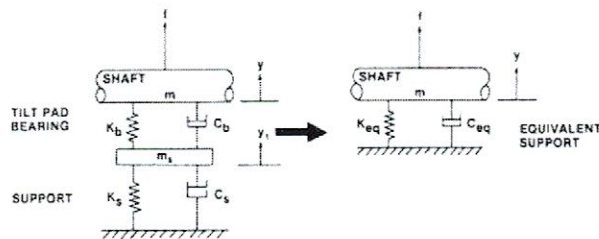

Figure 3. Single Degree of Freedom Flexible Support and Equivalent Support Model.

The Y displacement shown in Figure 3 is the absolute rotor response; Y_1 is the support or pedestal response and $Y - Y_1$ is the relative rotor response. Since most vibration probes are mounted on the bearing case to monitor shaft motion, it is the relative response that is of primary importance for correlation purposes.

From Figure 3, the bearing stiffness and damping are combined with the support mass, stiffness, and damping to yield an equivalent support model. In this model, the bearing stiffness and damping, K_b and C_b, are functions of the shaft rotational speed, ω. The equivalent support properties are also speed dependent while the support stiffness and damping, K_s and C_s, may be constant or speed dependent. The details of combining the support and bearing properties for tilt pad bearings with no cross-coupling terms are shown in the Nicholas and Barrett study [2] and herein in the APPENDIX. The support cross-coupling is also set to zero. Bearing cross-coupling can easily be incorporated into the model, but inclusion of the support cross-

coupling makes the equations too cumbersome. However, the modelling technique outlined by Barrett, Nicholas and Dhar [3] can easily consider support cross-coupling in the horizontal-vertical (X,Y) directions as well as cross-coupling from one support to another.

To summarize, the bearing oil film stiffness and damping properties are calculated with or without the effect of pad and/or pivot flexibility. These characteristics are then combined with the SDOF support systems' stiffness, mass, and damping properties via the equations in the APPENDIX. These calculations yield equivalent stiffness and damping coefficients that may then be used directly in rotordynamic response and stability computer programs.

DETERMINING DYNAMIC SUPPORT STIFFNESS

Test Procedure

In order to determine the stiffness and damping properties of an actual bearing support, a modal or spectral analyzer is utilized. A block diagram of the test system is illustrated in Figure 4. An impact hammer is used to excite the bearing case at the bearing centerline. An internal load cell registers the force imparted on the bearing case by the hammer. Mounted on the case at the bearing centerline is an accelerometer that senses the bearing case motion that results from the impact force. The modal analyzer double integrates the acceleration and divides the resulting displacement by the force from the impact hammer. This integration and division, calculated over a specified frequency range, is the compliance FRF, which is complex, containing both amplitude and phase information.
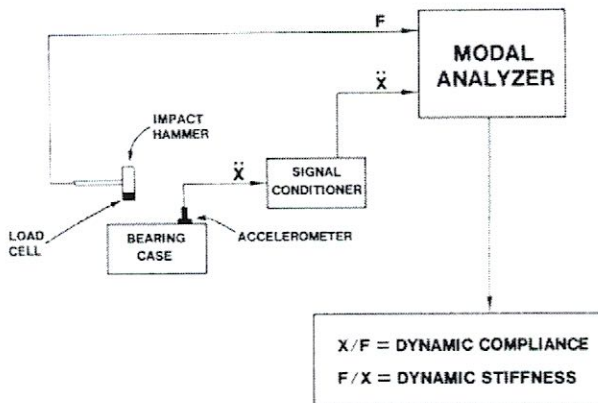

Figure 4. Modal Analysis Schematic Diagram.

Example compliance FRF plots are shown in Figures 5 and 6 for a steam turbine case. The exhaust end vertical compliance (Figure 5) results from a vertically mounted accelerometer sensing vertical acceleration from a vertical excitation (principal compliance). Likewise, the vertical principal compliance for the steam end bearing case is shown in Figure 6. In both figures, two different excitation sources are shown: an impact hammer and an electromagnetic exciter or shaker. Note that for frequencies below 200 Hz (12000 cpm), both excitation sources give very nearly identical results. The impact hammer offers the advantage of being significantly quicker to set up and conduct the actual modal testing.

The compliance plots in Figures 5 and 6 are the magnitude of the complex compliance FRF. The corresponding FRF phase angle for the exhaust end bearing case is plotted in Figure 7 for the vertical direction. Both magnitude and phase are necessary to determine the support flexibility parameters used in the support model. Details of this procedure are discussed later.
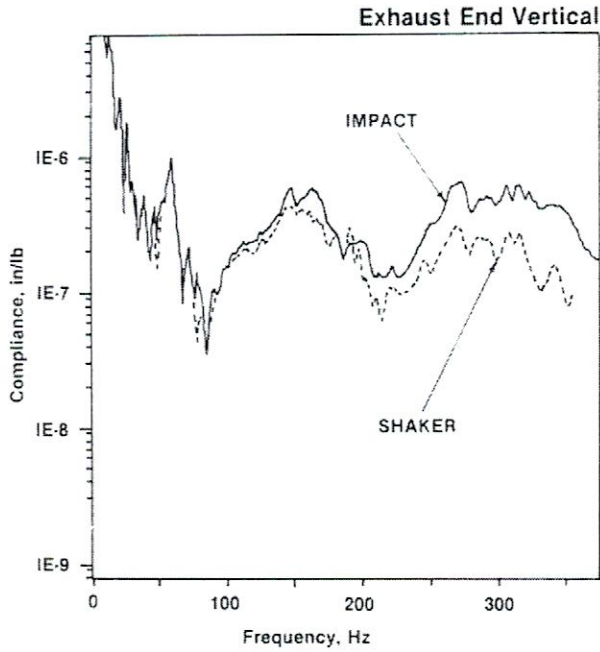
4

Exhaust End Vertical

Figure 5. Compliance FRF Plots Comparing Shaker and Impact Excitation—Exhaust End Vertical.
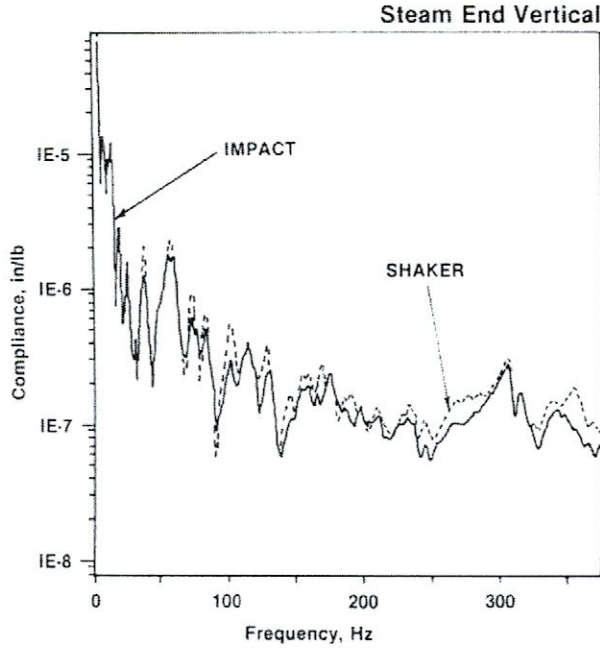
Steam End Vertical

Figure 6. Compliance FRF Plots Comparing Shaker and Impact Excitation—Steam End Vertical.

Analytical Calculations

Since the support model discussed previously (see APPENDIX and Figure 3) uses two SDOF spring-mass-damper systems per bearing case, it is appropriate to examine the compliance FRF for a SDOF system [13].
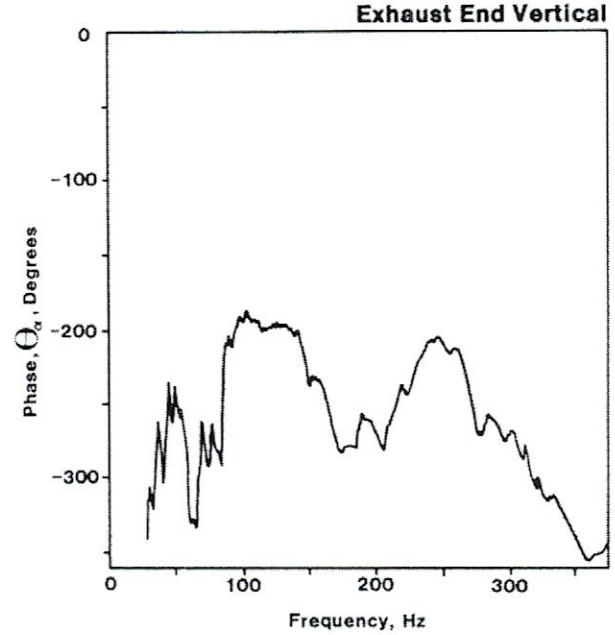
Exhaust End Vertical

Figure 7. FRF Phase Angle, Impact Excitation—Exhaust End Vertical.

$$\alpha(\omega) = \frac{1}{(K_s - m_s\omega^2) + i\,(C_s\omega)} \quad (1)$$

The magnitude of the complex compliance of Equation (1) is

$$|\alpha(\omega)| = \frac{|X|}{|F|} = \frac{1}{\sqrt{(K_s - m_s\omega^2)^2 + (C_s\omega)^2}} \quad (2)$$

where

F = applied force
X = resulting displacement

inverting,

$$K_d = \frac{|F|}{|X|} = \sqrt{(K_s - m_s\omega^2)^2 + (C_s\omega)^2} \quad (3)$$

where K_d is the magnitude of the dynamic stiffness.
The phase angle is [13]

$$\angle\alpha(\omega) = \angle X - \angle F = -\theta_\alpha = \tan^{-1}\left(\frac{-C_s\omega}{K_s - m_s\omega^2}\right) \quad (4)$$

let
$$\hat{K}_s = K_s - m_s\omega^2 \quad (5)$$
$$\hat{C}_s = C_s\omega$$

thus
$$K_d^2 = \hat{K}_s^2 + \hat{C}_s^2 \quad (6)$$
$$\tan\theta_\alpha = \hat{C}_s/\hat{K}_s$$

Or

$$\hat{K}_s^2 = \frac{K_d^2}{1 + \tan^2\theta_\alpha} \quad (7)$$
$$\hat{C}_s^2 = K_d^2 - \hat{K}_s^2$$

Thus, the real and imaginary parts of the FRF may be calculated from Equation (7) and used directly in the flexible support model derived in the APPENDIX. The dynamic support stiffness, K_d, is the inverse of the compliance from plots such as those depicted later in Figures 11 and 12. The phase angle, Θ_α, is obtained from the phase versus frequency plot such as in Figure 7. From Equation (7), $\acute{K}_s$ is equivalent to Equations (A-13) and (A-14) while $\acute{C}_s$ gives the support damping used in Equations (A-9) through (A-12).

FORCED RESPONSE CORRELATION

Test Stand Results

A nine stage 2418 pound steam turbine rotor was tested with 23 ounce-inches of unbalance placed at the center wheel rim. The rotor, operating on five pad tilting pad bearings with 5.0 in and 4.0 in diameter journals on the exhaust and steam ends, was run up to a trip speed of 6150 cpm.

The resulting speed-amplitude plots are shown in Figure 8 (exhaust end probes) and Figure 9 (steam end probes). The probes, which are mounted on both bearing cases, are clocked 45 degrees from top dead center and are referred to as "right probe" and "left probe."

From Figures 8 and 9, the left probe shows a split first critical speed at 3000 and 3150 cpm while the right probe indicates a 2700 cpm to 3200 cpm split critical. Smaller sub-peaks, which are thought to be support resonances, also exist at 1700 cpm, 2500 cpm, and 3600 cpm.
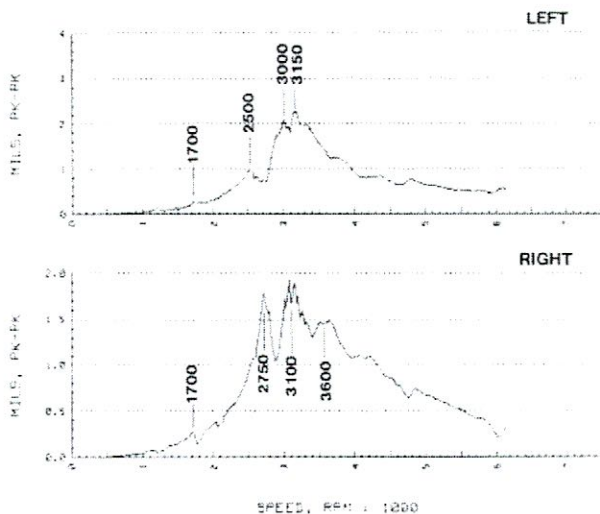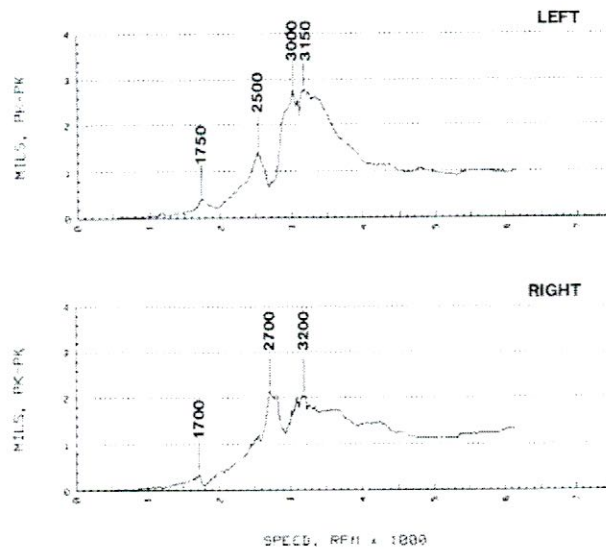

MEASURED ROTOR AMPLITUDE
EXHAUST END PROBES

Figure 8. Steam Turbine Test Stand Speed-Amplitude Plots, Exhaust End Probes.

Rigid Support Analysis

The analytical results from a forced response analysis assuming rigid supports for the exhaust end probes are plotted in Figure 10 for the exhaust end probes. The predicted first critical speed is 3250 cpm for the left probe and 3400 cpm for the right probe. While these values range from 100 cpm to 700 cpm high, the rigid support analysis fails to predict the split first critical or any of the support resonances.

Flexible Support Analysis—Constant Stiffness

The simplest flexible support model that can be employed is to use the identical spring-mass-damper support system over

MEASURED ROTOR AMPLITUDE
STEAM END PROBES

Figure 9. Steam Turbine Test Stand Speed-Amplitude Plots, Steam End Probes.
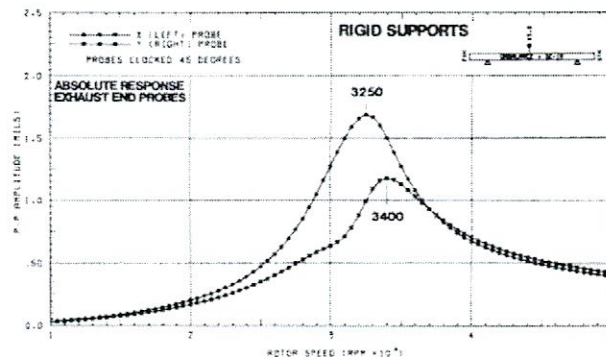

Figure 10. Analytical Results, Rigid Support Model, Exhaust End Probes.

the entire speed range, for both bearing cases and for both the horizontal and vertical directions [2]. Values for the spring-mass-damper system can be calculated from the compliance FRF plots. The plots for the exhaust end bearing case are shown in Figures 11 and 12. Recall that the inverse of the compliance plotted in Figures 11 and 12 is the dynamic stiffness, K_d. From Equation (3), the dynamic stiffness contains not only the support stiffness, K_s, but also the support mass, m_s, and the support damping, C_s. However, it is clear that K_s and m_s need not be determined explicitly as $\acute{K}_s$, Equation (5), contains both K_s and m_s, and $\acute{K}_s$ may be used directly in the equivalent support model, Equations (A-9) through (A-14).

The dynamic stiffness, K_d, is picked off of Figures 11 and 12 at 3000 cpm (near the critical speed in question). While it is not necessary, for simplicity, an average value of $K_d = 1.5 \times 10^6$ lbs/in is used. The dynamic compliance plots for the steam end bearing case are also considered in the averaging.

While the phase angle can be utilized along with Equations (5) and (7) to calculate the support damping, C_s, this method is not
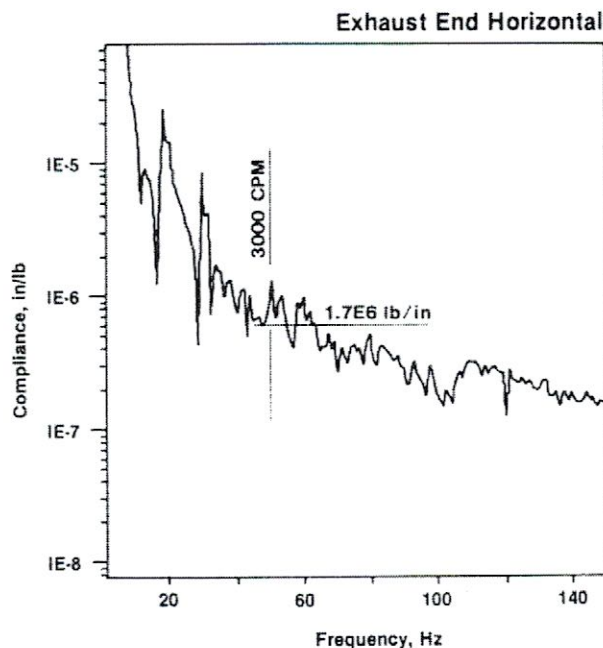
Exhaust End Horizontal

Figure 11. *Compliance FRF Data, Constant Stiffness Support Model—Exhaust End Horizontal.*
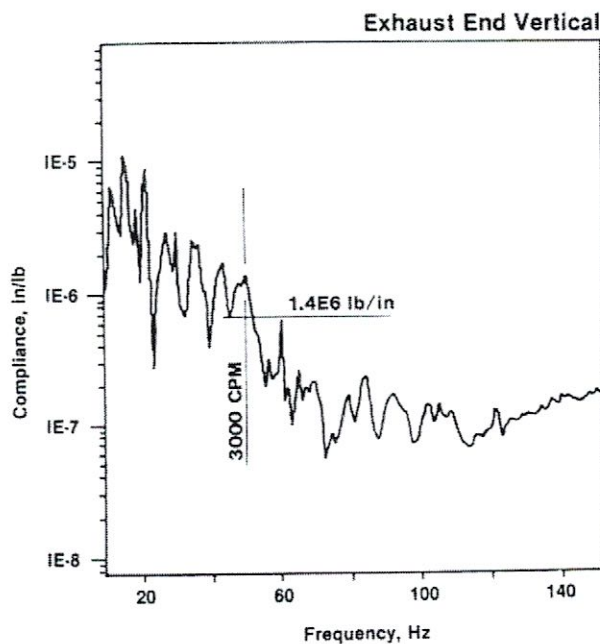
Exhaust End Vertical

Figure 12. *Compliance FRF Data, Constant Stiffness Support Model—Exhaust End Vertical.*

used here. Instead, and again for simplicity, ten percent of the critical damping is assumed [2].

With K_d averaged at 3000 cpm from the dynamic compliance plots and with C_s as calculated earlier, $\hat{K}_s$ may be solved for from Equations (3) and (5).

$$\hat{K}_s = \sqrt{K_d{}^2 - (C_s\omega)^2} \qquad (8)$$

Thus, with $\hat{K}_s$ and C_s known and set equal in the horizontal-vertical (X,Y) directions for both bearing cases, the equivalent support stiffness and damping properties may be calculated from equations (A-9) through (A-14).

The results of the forced response analysis using this constant stiffness model is shown in Figure 13 where the rotor response relative to the exhaust end probes is plotted. The critical speeds are now predicted at 2925 cpm (left probe) and 3050 cpm (right probe). These values fall within the actual critical speeds discussed previously (2700 cpm to 3200 cpm). However, this model does not predict the split criticals or any of the support resonances.
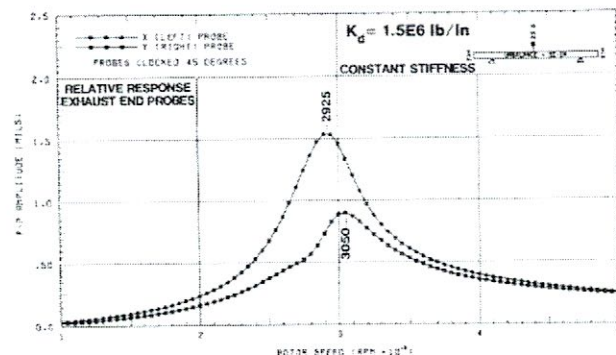

Figure 13. *Analytical Results, Constant Stiffness Support Model, Relative Response—Exhaust End Probes.*

The constant stiffness model may be easily refined by using the actual K_d values from each of the four dynamic compliance plots instead of using an average value. Also, the phase plots may be employed to calculate C_s, instead of simply using ten percent of critical damping. But, these refinements will not show the support resonances as the model is accurate only in the vicinity of 3000 cpm.

This type of constant stiffness model (refined or unrefined) has been successful in accurately predicting the location and amplification of the first and second critical speeds [2]. Different models should be used for each critical in question as the dynamic compliance can be significantly different in the vicinity of the first critical speed compared to the second or third critical speeds. Thus, separate forced response runs should be made with the different SDOF support models to locate each critical speed.

Flexible Support Analysis—Dynamic Compliance Model

In an attempt to predict the split critical peaks and support resonance speeds of Figures 8 and 9, a more sophisticated model is devised where multiple SDOF spring-mass-damper systems are used to represent the supports over the entire speed range. The model approximations are illustrated in Figures 14 and 15 on the steam end compliance FRF curves. As indicated in the figures, the dynamic compliance curves are approximated as a series of straight lines. The dynamic stiffness along with the frequency is tabulated for all points where the straight lines intersect. These data are then used as flexible support input parameters in the forced response computer program.

Thus, a different SDOF spring-mass-damper support system is used for every speed increment in the response program. Linear interpolation is used for all speeds between the input speeds. A similar set of data can be tabulated for the phase angle. With K_d and Θ_α specified as input, K_s and C_s can be calculated from Equations (5) and (7) and, along with the speed dependent bearing characteristics, equivalent support values calculated for any speed from Equations (A-9) through (A-14).
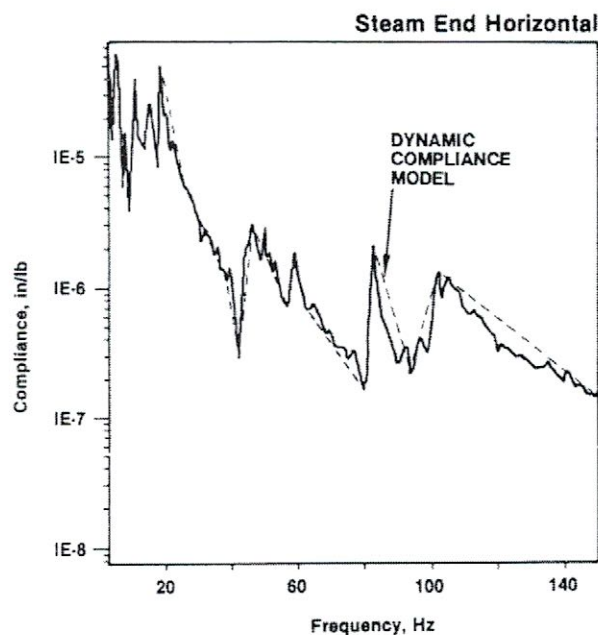
Steam End Horizontal

Figure 14. Compliance FRF Data, Dynamic Compliance Support Model—Steam End Horizontal.
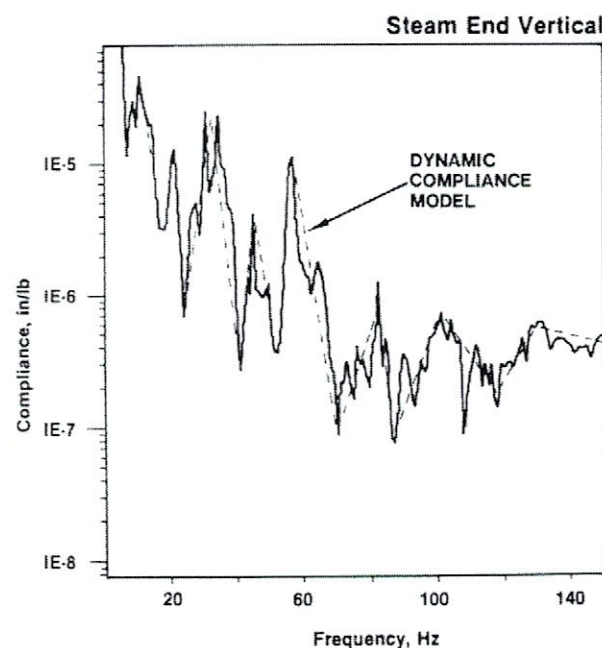
Steam End Vertical

Figure 15. Compliance FRF Data, Dynamic Compliance Support Model—Steam End Vertical.

As in the previous flexible support model, the phase angle is not used here to determine C_s. Instead, for simplicity, ten percent of the critical damping is assumed for C_s. Forced response plots using this dynamic compliance model are shown in Figures 16, 17, and 18.

A plot of the *absolute* response for the steam end probe is presented in Figure 16. Predicted criticals are at 3050 cpm for the left probe. Twin peaks occur at 2750 cpm and 3750 cpm for the right probe.
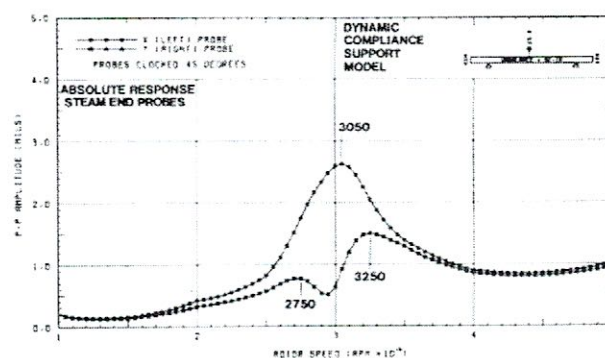

Figure 16. Analytical Results, Dynamic Compliance Support Model, Absolute Response—Steam End Probes.
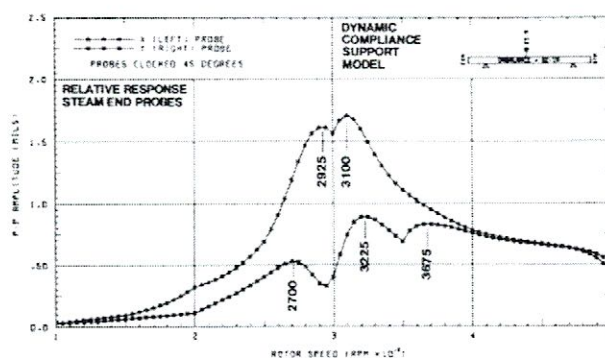

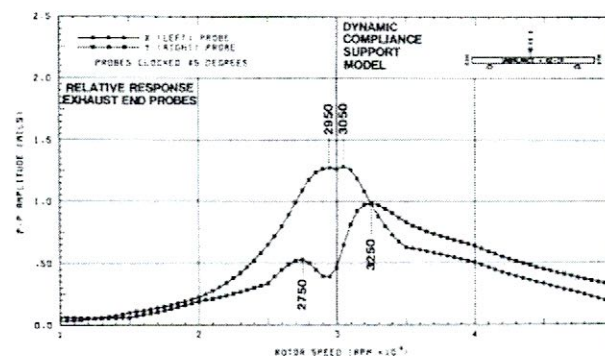Figure 17. Analytical Results, Dynamic Compliance Support Model, Relative Response—Steam End Probes.

Figure 18. Analytical Results, Dynamic Compliancce Support Model, Relative Response—Exhaust End Probes.

The *relative* probe-to-shaft response is shown in Figures 17 and 18. The steam end response (Figure 17) predicts a split critical for the left probe at 2925 cpm and 3100 cpm, which correlates very closely to the actual values of 3000 cpm and 3150 cpm from Figure 9. The predicted right probe split critical peaks are at 2700 cpm and 3225 cpm, with a support resonance peak at 3675 cpm. Actual right probe split critical peaks are at 2700 cpm and 3200 cpm. The predicted 3675 cpm support resonance is more evident in Figure 8 on the right exhaust end probe, where the actual support resonance speed is 3600 cpm.

For the exhaust end, split peaks are predicted for the left probe at 2950 cpm and 3050 cpm, compared to actual values of 3000 cpm and 3150 cpm from Figure 8. Split first critical peaks are predicted at 2750 cpm and 3250 cpm for the right probe, while actual values are 2750 cpm and 3100 cpm.

Flexible Support Analysis—FRF Data

In the previous section, a limited number of straight lines were used to approximate the compliance FRF curve. Between 12 and 20 data points were used as input data to the response program. While this dynamic compliance model provided excellent results, some support resonance peaks, such as the 1700 cpm, were still not predicted. It is clear that more data points are necessary.

Barrett, Nicholas and Dhar [3] attempted to correlate the actual response curves for the same turbine, using a flexible support modelled directly from the compliance FRF curve. Over 50 FRF data points were used from a tabular FRF output.

Results from the FRF support model are plotted in Figure 19 for the steam end right probe's relative response. Note that the 1700 cpm support resonance is predicted along with a smaller resonance at 1300 cpm. The minor 1300 cpm peak is barely evident at 1200 cpm in Figures 8 and 9. This model also predicts the split first critical speed.
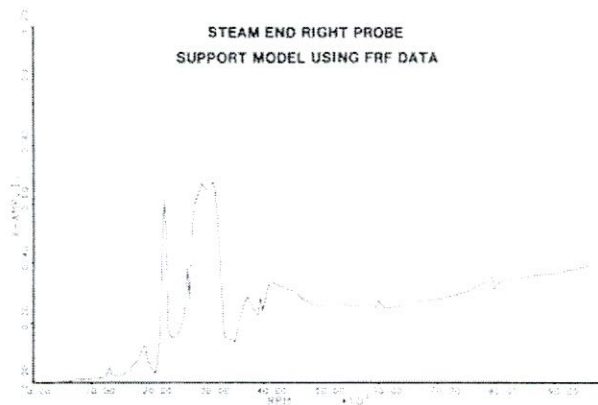

STEAM END RIGHT PROBE
SUPPORT MODEL USING FRF DATA

Figure 19. Analytical Results, FRF Support Model, Relative Response—Steam End Right Probe.

DISCUSSION OF RESULTS

While a procedure for determining the support damping from the compliance FRF data is discussed, it is not used herein. Instead, the amount of support damping is simply approximated as ten percent of the critical damping. The problem with using the FRF phase angle to determine C_s is that the phase angle, and thus, the support damping, is the least reliable information attainable from experimental modal analysis techniques.

When the support resonances are few, well defined and well separated, circle fitting techniques are normally employed to determine C_s [13]. However, this is impossible with the types of complex support systems usually found in the rotating machinery industry. The entire supporting structure, including the associated piping, contributes to the complex FRF curve with many resonances spaced very close together.

It is generally agreed that the support damping is small and even ten percent of the critical damping is probably too much. This is evident by comparing the relative analytical response curves to the actual curves. The unbalance used to excite the rotor in the analytical forced response analysis is identical to the unbalance used in the shop test. However, the analytical response at the critical peaks is consistently predicted lower than the actual values. Actual peak vibration levels range from 2.8 to 2.0 mils (Figures 8 and 9), while predicted *relative* response levels using the dynamic compliance support model range from 1.75 to 0.9 mils (Figures 17 and 18). *Absolute* response results using the same support model from Figure 16 show better peak vibration correlation, as the peak vibration for

the steam end left probe is 2.6 mils. These comparisons seem to indicate that ten percent of the critical damping overestimates the amount of actual structural damping available in the real system.

It is also clear that examination of the *relative* probe-to-shaft analytical response is necessary. The absolute response of Figure 16 does not show the split critical peaks for the left probe or the predicted 3675 cpm support resonance. However, split peaks for both probes as well as several support resonances are evident from the analytical relative response curves of Figures 17, 18, and 19.

CONCLUSIONS

• Modelling each bearing support as two SDOF systems and utilizing impact hammer compliance FRF data produces excellent analytical forced response correlation with actual test stand results.

• Using the constant stiffness model, the location of the first critical speed is accurately predicted. However, the split critical peaks and the numerous support resonances are not evident from the analysis.

• Using many SDOF spring-mass-damper systems over the operating speed range (dynamic compliance model) results not only in an accurate first critical speed prediction, but the split critical peaks are also evident along with one of the support resonances.

• Using 50 data points from the FRF compliance curves results in the prediction of two more support resonance speeds.

• With the support damping approximated at ten percent of the critical damping, accurate predictions of the location of the rotor and support resonance speeds along with split critical peaks are possible. However, the amplitude of vibration is lower than actual values.

NOMENCLATURE

$\hat{C}_s$	$C_s\omega$ (FL^{-1})
C_b, C_s, C_{eq}	bearing, support, equivalent support damping (FTL^{-1})
$C_{xx}, C_{yy}, C_{eqxx}, C_{eqyy}$	bearing, equivalent support principal damping (FTL^{-1})
C_{sx}, C_{sy}	horizontal, vertical support damping (FTL^{-1})
F', f	unbalance force (F)
F	applied force for FRF (F)
g	gravitational constant (LT^{-2})
K_d	$(\hat{K}_s^2 + \hat{C}_s^2)^{1/2}$, dynamic support stiffness (FL^{-1})
K_b, K_s, K_{eq}	bearing, support, equivalent support stiffness (FL^{-1})
$\hat{K}_s$	$K_s - m_s\omega^2$ (FL^{-1})
$K_{xx}, K_{yy}, K_{eqxx}, K_{eqyy}$	bearing, equivalent support principal stiffness (FL^{-1})
K_{sx}, K_{sy}	horizontal, vertical support stiffness (FL^{-1})
m, m_s	journal, support mass (FT^2L^{-1})
m_{sx}, m_{sy}	horizontal, vertical support mass (FT^2L^{-1})
t	time (T)
X, Y	horizontal, vertical coordinates
X	resulting FRF displacement (L)
$\ddot{X}$	resulting FRF acceleration (LS^{-2})
$\alpha(\omega)$	compliance frequency response function, FRF (LF^{-1})

θ_α phase angle of $\alpha(\omega)$, (degrees)

ω rotational speed (rad/sec)

APPENDIX

For the shaft-bearing-support system of Figure 3, the equations of motion are [2]

$$m\ddot{y} + C_b(\dot{y} - \dot{y}_1) + K_b(y - y_1) = f \tag{A-1}$$

$$m_s\ddot{y}_1 + C_s\dot{y}_1 + C_b(\dot{y}_1 - \dot{y}) + K_s y_1 + K_b(y_1 - y) = 0 \tag{A-2}$$

Assuming synchronous forced response at frequency ω,

$$y = Ye^{i\omega t} \qquad y_1 = Y_1\,e^{i\omega t} \qquad f = F'_e\,e^{i\omega t}$$

Equation (A-2) becomes

$$(\hat{K}_s + K_b + i\omega C_s + i\omega C_b)Y_1 = (K_b + i\omega C_b)Y \tag{A-3}$$

Where, for simplicity $\hat{K}_s = K_s - m_s\omega^2$

Equation (A-1) becomes

$$F' = K_b Y - K_b Y_1 + i\omega\,(C_b Y - C_b Y_1) - m\omega^2 Y \tag{A-4}$$

Solving for Y_1 in (A-3) and substituting into (A-4) yields

$$F' = \left[K_b - \frac{K_b^2 + i\omega C_b K_b}{\hat{K}_s + K_b + i\omega(C_s + C_b)} \right] Y$$
$$+ i\omega \left[C_b - \frac{K_b C_b + i\omega C_b^2}{\hat{K}_s + K_b + i\omega(C_s + C_b)} \right] Y - m\omega^2\,Y \tag{A-5}$$

For the equivalent system

$$F' = K_{eq}Y + i\omega C_{eq}Y - m\omega^2 Y \tag{A-6}$$

Combining (A-5) and (A-6), rationalizing and simplifying yields the equivalent support stiffness and damping properties.

$$K_{eq} = \frac{\hat{K}_s K_b(\hat{K}_s + K_b) + \omega^2(K_b C_s^2 + \hat{K}_s C_b^2)}{(\hat{K}_s + K_b)^2 + \omega^2(C_s + C_b)^2} \tag{A-7}$$

$$C_{eq} = \frac{K_b^2 C_s + \hat{K}_s^2 C_b + \omega^2 C_s C_b(C_s + C_b)}{(\hat{K}_s + K_b)^2 + \omega^2(C_s + C_b)^2} \tag{A-8}$$

From equations (A-7) and (A-8), four principal stiffness and damping coefficients may be written for the equivalent support system.

$$K_{eqxx} = \frac{\hat{K}_{sx}K_{xx}(\hat{K}_{sx} + K_{xx}) + \omega^2(K_{xx}C_{sx}^2 + \hat{K}_{sx}C_{xx}^2)}{(\hat{K}_{sx} + K_{xx})^2 + \omega^2(C_{sx} + C_{xx})^2} \tag{A-9}$$

$$K_{eqyy} = \frac{\hat{K}_{sy}K_{yy}(\hat{K}_{sy} + K_{yy}) + \omega^2(K_{yy}C_{sy}^2 + \hat{K}_{sy}C_{yy}^2)}{(\hat{K}_{sy} + K_{yy})^2 + \omega^2(C_{sy} + C_{yy})^2} \tag{A-10}$$

$$C_{eqxx} = \frac{K_{xx}^2 C_{sx} + \hat{K}_{sx}^2 C_{xx} + \omega^2 C_{sx}C_{xx}(C_{sx} + C_{xx})}{(\hat{K}_{sx} + K_{xx})^2 + \omega^2(C_{sx} + C_{xx})^2} \tag{A-11}$$

$$C_{eqyy} = \frac{K_{yy}^2 C_{sy} + \hat{K}_{sy}^2 C_{yy} + \omega^2 C_{sy}C_{yy}(C_{sy} + C_{yy})}{(\hat{K}_{sy} + K_{yy})^2 + \omega^2(C_{sy} + C_{yy})^2} \tag{A-12}$$

with

$$\hat{K}_{sx} = K_{sx} - m_{sx}\omega^2 \tag{A-13}$$

$$\hat{K}_{sy} = K_{sy} - m_{sy}\omega^2 \tag{A-14}$$

Note that from Equations (A-13) and (A-14), it is not necessary to calculate the support mass explicitly as K_{xx} and K_{yy} are the real part of the FRF. The support damping C_{xx} and C_{yy} are the imaginary part of the FRF.

It is not mandatory to assume zero cross-coupling for the bearing fluid film (i.e., tilt pad bearings). However, for zero cross-coupling, the X and Y direction equations become uncoupled, and Equations (A-7) through (A-12) can be easily derived explicitly.

REFERENCES

1. American Petroleum Institute, "Special-Purpose Steam Turbines for Refinery Services," API Standard 612, Second Edition, (June 1979).

2. Nicholas, J. C., and Barrett, L. E., "The Effect of Bearing Support Flexibility on Critical Speed Prediction," ASLE Transactions, 29(3), (July 1986).

3. Barrett, L. E., Nicholas, J. C., and Dhar, D., "The Dynamic Analysis of Rotor-Bearing Systems Using Experimental Bearing Support Compliance Data," Proceedings of the 4th International Modal Analysis Conference, Union College, Schenectady, New York, II, pp. 1531-1535, (1986).

4. Lund, J. W., and Pedersen, L. B., "The Influence of Pad Flexibility on the Dynamic Coefficients of a Tilting Pad Journal Bearing," ASME Paper No. JAT6-03, (October 1986).

5. Bansal, P. N., and Kirk, R. G., "Stability and Damped Critical Speeds of Rotor-Bearing Systems," ASME Journal of Engineering for Industry, 94(4), pp. 1325-1332, (November 1975).

6. Hashish, E. and Sankar, T. C., "Finite Element and Modal Analyses of Rotor-Bearing Systems Under Stochastic Loading Conditions," ASME Journal of Vibration, Acoustics, Stress, and Reliability in Design, 106(1), pp. 80-89 (January 1984).

7. Kirk, R. G., and Gunter, E. J., "The Effect of Support Flexibility and Damping on the Synchronous Response of a Single Mass Flexible Rotor," ASME Journal of Engineering for Industry, 94(1), (February 1972).

8. Lund, J. W., "The Stability of an Elastic Rotor in Journal Bearings with Flexible, Damped Supports," ASME Journal of Applied Mechanics, 87, Series E, pp. 911-920, (December 1965).

9. Gunter, E. J., Li, D. F., and Barrett, L. E., "Unbalance Response of a Two Spool Gas Turbine Engine with Squeeze Film Bearings," ASME Paper No. 81-GT-219 (1981).

10. Li, D. F., and Gunter, E. J., "Component Mode Synthesis of Large Rotor Systems," ASME Journal of Engineering for Power, 104(2), pp. 552-560 (1982).

11. Glasgow, D. A., and Nelson, H. D., "Stability Analysis of Rotor Systems Using Component Mode Synthesis," ASME Journal of Mechanical Design, 102(2), pp. 352-359 (April 1980).

12. Queitzsch, G. K., "Forced Response Analysis of Multi-Level Rotor Systems with Substructure," Ph.D. Dissertation, University of Virginia (January 1985).

13. Ewins, D. J., *Modal Testing: Theory and Practice*, Letchworth, Hertfordshire, England: Research Studies Press, (1984).

14. Caruso, W. J., Gaus, B. E., and Catlow, W. G., "Application of Recent Rotor Dynamics Developments to Mechanical Drive Turbines," *Proceedings of the Eleventh Turbomachinery Symposium*, Turbomachinery Laboratories, Department of Mechanical Engineering, Texas A&M University, College Station, Texas, pp. 1-17, (1982).

15. Vance, J. M., Murphy, B. T., and Tripp, H. A., "Critical Speeds of Turbomachinery: Computer Predictions vs. Experimental Measurements—Part II: Effect of Tilt-Pad Bearings and Foundation Dynamics," ASME Preprint 85-DET-146 (September 1985).

RMT™

ROTATING MACHINERY TECHNOLOGY

4181 BOLIVAR ROAD
WELLSVILLE, NY 14895
585-593-3700 (VOICE)
585-593-2693 (FAX)

www.rmt-inc.com
jcn@rmt-inc.com